

Convergence Analysis and Numerical Implementation of a Second Order Numerical Scheme for the Three-Dimensional Phase Field Crystal Equation

Lixiu Dong^{*} Wenqiang Feng[†] Cheng Wang[‡] Steven M. Wise[§] Zhengru Zhang[¶]

November 22, 2016

Abstract

In this paper we analyze and implement a second-order-in-time numerical scheme for the three-dimensional phase field crystal (PFC) equation. The numerical scheme was proposed in [46], with the unique solvability and unconditional energy stability established. However, its convergence analysis remains open. We present a detailed convergence analysis in this article, in which the maximum norm estimate of the numerical solution over grid points plays an essential role. Moreover, we outline the detailed multigrid method to solve the highly nonlinear numerical scheme over a cubic domain, and various three-dimensional numerical results are presented, including the numerical convergence test, complexity test of the multigrid solver and the polycrystal growth simulation.

Keywords: three-dimensional phase field crystal, finite difference, energy stability, second order numerical scheme, convergence analysis, nonlinear multigrid solver

1 Introduction

Defects, such as vacancies, grain boundaries, and dislocations, are observed in crystalline materials, and a precise and accurate understanding of their formation and evolution is of great interest. The phase field crystal (PFC) model was proposed in [25] as a new approach to simulate crystal dynamics at the atomic scale in space but on diffusive scales in time. This model naturally incorporates elastic and plastic deformations, multiple crystal orientations and defects and has already been used to simulate a wide variety of microstructures, such as epitaxial thin film growth [24], grain growth [57], eutectic solidification [27], and dislocation formation and motion [52, 57]. The idea is that the phase variable describes a coarse-grained temporal average of the number density of atoms, and

^{*}School of Mathematical Sciences, Beijing Normal University, Beijing 100875, P.R. China (201421130036@mail.bnu.edu.cn)

[†]Department of Mathematics, The University of Tennessee, Knoxville, TN 37996 (Corresponding Author: wfeng1@utk.edu)

[‡]Department of Mathematics, The University of Massachusetts, North Dartmouth, MA 02747 (cwang1@umassd.edu)

[§]Department of Mathematics, The University of Tennessee, Knoxville, TN 37996 (swise@math.utk.edu)

[¶]School of Mathematical Sciences, Beijing Normal University, Beijing 100875, P.R. China (zrzhang@bnu.edu.cn)

the approach can be related to dynamic density functional theory [6, 48]. The method represents a significant advantage over other atomistic methods, such as molecular dynamics methods where the time steps are constrained by atomic-vibration time scales. More detailed descriptions are available in [1, 2, 3, 7, 10, 11, 26, 44, 49, 50, 51, 53, 54, 57, 58, 67, 71, 72, 76], and the related works for the amplitude expansion approach could be found in [4, 26, 33, 34, 37, 56, 75].

Consider the dimensionless energy of the form [24, 25, 59]:

$$E(\phi) = \int_{\Omega} \left[\frac{1}{4}\phi^4 + \frac{1-\epsilon}{2}\phi^2 - |\nabla\phi|^2 + \frac{1}{2}(\Delta\phi)^2 \right] d\mathbf{x}, \quad (1.1)$$

where $\Omega = (0, L_x) \times (0, L_y) \times (0, L_z) \subset \mathbb{R}^3$, $\phi : \Omega \rightarrow \mathbb{R}$ is the atom density field, and $\epsilon > 0$ is a constant. We assume that ϕ is periodic on Ω . This model naturally incorporates elastic and plastic deformation of the crystal and the various crystal defects. The PFC equation [24, 25] is given by the H^{-1} gradient flow associated with the energy (1.1):

$$\begin{aligned} \phi_t &= \nabla \cdot (M(\phi)\nabla\mu), \quad \text{in } \Omega_T = \Omega \times (0, T), \\ \mu &= \delta_{\phi}E = \phi^3 + (1-\epsilon)\phi + 2\Delta\phi + \Delta^2\phi, \quad \text{in } \Omega_T, \\ \phi(x, y, z, 0) &= \phi_0(x, y, z), \quad \text{in } \Omega. \end{aligned} \quad (1.2)$$

in which $M(\phi) > 0$ is a mobility, μ is the chemical potential. Periodic boundary conditions are imposed for ϕ , $\Delta\phi$ and μ .

The PFC equation is a high-order (sixth-order) nonlinear partial differential equation. There have been some related works to develop numerical schemes for the PFC equation. Cheng and Warren [18] introduced a linearized spectral scheme, similar to one for the Cahn-Hilliard equation analyzed in [63]. This scheme is not expected to be provably unconditionally energy stable. The finite element PFC method of Backofen *et al.* [6] employs what is essentially a standard backward Euler scheme, but where the nonlinear term ϕ^3 in the chemical potential is linearized via $(\phi^{k+1})^3 \approx 3(\phi^k)^2\phi^{k+1} - 2(\phi^k)^3$. Both energy stability and solvability are issues for this scheme, because the term $2\Delta\phi$ is implicit in the chemical potential. Tegze *et al.* [60] developed a semi-implicit spectral scheme for the binary PFC equations that is not expected to be unconditionally stable. Also see other related numerical works [5, 13, 42, 45] in recent years.

The energy stability of a numerical scheme has always been a very important issue, since it plays an essential role in the accuracy of long time numerical simulation. The standard convex splitting scheme, originated from Eyre's work [28], has been a well-known approach to achieve numerical energy stability. In this framework, the convex part of the chemical potential is treated implicitly, while the concave part is updated explicitly. A careful analysis leads to the unique solvability and unconditional energy stability of the numerical scheme, unconditionally with respect to the time and space step sizes. Such an idea has been applied to a wide class of gradient flows in recent years, and both first and second order accurate in time algorithms have been developed. See the related works for the PFC equation and the modified PFC (MPFC) equation [8, 9, 12, 36, 46, 65, 66, 69]; the epitaxial thin film growth models [14, 17, 55, 64]; Cahn-Hilliard equation [23, 41]; non-local Cahn-Hilliard-type models [38, 39], the Cahn-Hilliard-Hele-Shaw (CHHS) and related models [15, 16, 20, 22, 32, 68], etc.

On the other hand, a well-known drawback of the first order convex splitting approach is that an extra dissipation has been added to ensure unconditional stability; in turn, the first order numerical

approach introduces a significant amount of numerical error [19]. For this reason, second-order energy stable methods have been highly desirable.

There have been other related works of “energy stable” schemes for the certain gradient flows in recent years. For example, an alternate variable is used in [40], denoted as a second order approximation to $v = \phi^2 - 1$ in the Cahn-Hilliard model. A linearized, second order accurate scheme is derived as the outcome of this idea, and the stability is established for a modified energy. A similar idea has been applied to the PFC model in a more recent article [74]. However, such an energy stability is applied to a pair of numerical variables (ϕ, v) , and an H^2 stability for the original physical variable ϕ has not been justified. As a result, the convergence analysis is not available for this numerical approach. Similar methodology has been reported in the invariant energy quadratization (IEQ) approach [43, 73, 78], etc.

In comparison, a second order numerical scheme was proposed and studied for the PFC equation in [46]. By a careful choice of the second order temporal approximations to each term in the chemical potential, the unique solvability and unconditional energy were justified at a theoretical level, with the centered difference discretization taken in space. In particular, this energy stability is derived with respect to the original energy functional, combined with an auxiliary, non-negative correction term, so that a uniform in time H^2 bound is available for the numerical solution. Meanwhile, a detailed convergence analysis has not been theoretically reported for the proposed second order scheme, although the full convergence order was extensively demonstrated in the numerical experiments. The key difficulty in the convergence analysis is associated with the maximum norm bound estimate for the numerical solution, and such a bound plays an essential role in the theoretical convergence derivation. In more details, the unconditional energy stability indicates a uniform in time H^2 bound of the numerical solution at a discrete level. Although the Sobolev embedding from H^2 to L^∞ is straightforward in three-dimensional space, a direct estimate for the corresponding grid function is not directly available. In two-dimensional space, such a discrete Sobolev embedding has been proved in the earlier works [46, 69], using a complicated calculations of the difference operators. However, as stated in Remark 12 of [46], *“the proof presented in [69] does not automatically extend to three dimensions. This is because a discrete Sobolev inequality is used to translate energy stability into point-wise stability, and the inequality fails in three dimensions. We are currently studying the three dimensional case in further detail.”*

In this paper, we provide a detailed convergence analysis for the fully discrete scheme formulated in [46], which is shown to be second order accurate in both time and space. In particular, the maximum norm estimate of the three-dimensional numerical solution is accomplished via a discrete Fourier transformation over a uniform numerical grid, so that the discrete Parseval equality is valid. And also, the equivalence between the discrete and continuous H^2 norms for the numerical grid function and its continuous version, respectively, can be established. In turn, the discrete Sobolev inequality is obtained from its continuous version. Such an ℓ^∞ bound of the discrete numerical solution is crucial, so that the convergence analysis could go through for the scheme. Moreover, the Crank-Nicholson approximation to the surface diffusion term poses another challenge in the convergence proof, since the diffusion coefficients at time steps t^{k+1} and t^k are equally distributed, in comparison with an alternate second order approximation reported in a few recent works [23, 41], in which the diffusion coefficients are distributed at time steps t^{k+1} and t^{k-1} , respectively. To overcome this difficulty, we have to perform an error analysis at time instant $t^{k+1/2}$, in combination

a subtle estimate for the numerical error in the concave diffusion term.

In addition, we also present various numerical simulation results of three-dimensional PFC model in this article. It is noted that most numerical results for the PFC equation reported in the existing literature are two-dimensional, or over a two-dimensional surface; see [8, 18, 21, 35, 46, 77], etc. For a gradient flow in which the nonlinear terms takes a form of ϕ^3 pattern, great efficiency and accuracy of the nonlinear multi-grid solver have been extensively demonstrated in the numerical experiments; see the related works [8, 20, 41, 46, 38, 39, 68]. We apply the nonlinear multi-grid algorithm to implement the three-dimensional numerical scheme; its great numerical efficiency enables us to compute the three-dimensional model using local servers. Both the numerical accuracy check and the detailed numerical simulation results of three-dimensional polycrystal growth are reported.

The rest of paper is organized as follows. In Section 2, we introduce the finite difference spatial discretization in three-dimensional space, and review a few preliminary estimates. In Section 3 we review the second order numerical scheme proposed in [46], and state the main theoretical results. The detailed convergence proof is given by Section 4. Furthermore, the details of the three-dimensional multi-grid solver is outlined in Section 5. Subsequently, the numerical results are presented in Section 6. Finally, some concluding remarks are made in Section 7.

2 Finite difference discretization and a few preliminary estimates

For simplicity of presentation, we denote (\cdot, \cdot) as the standard L^2 inner product, and $\|\cdot\|$ as the standard L^2 norm, and $\|\cdot\|_{H^m}$ as the standard H^m norm. We use the notation and results for some discrete functions and operators from [41, 68, 70]. Let $\Omega = (0, L_x) \times (0, L_y) \times (0, L_z)$, where for simplicity, we assume $L_x = L_y = L_z =: L > 0$. It is also assumed that $h_x = h_y = h_z = h$ and we denote $L = m \cdot h$, where m is a positive integer. The parameter $h = \frac{L}{m}$ is called the mesh or grid spacing. We define the following two uniform, infinite grids with grid spacing $h > 0$:

$$E := \{x_{i+\frac{1}{2}} \mid i \in \mathbb{Z}\}, \quad C := \{x_i \mid i \in \mathbb{Z}\},$$

where $x_i = x(i) := (i - \frac{1}{2}) \cdot h$. Consider the following 3D discrete periodic function spaces:

$$\begin{aligned} \mathcal{C}_{\text{per}} &:= \{\nu : C \times C \times C \rightarrow \mathbb{R} \mid \nu_{i,j,k} = \nu_{i+\alpha m, j+\beta m, k+\gamma m}, \forall i, j, k, \alpha, \beta, \gamma \in \mathbb{Z}\}, \\ \mathcal{E}_{\text{per}}^x &:= \left\{ \nu : E \times C \times C \rightarrow \mathbb{R} \mid \nu_{i+\frac{1}{2}, j, k} = \nu_{i+\frac{1}{2}+\alpha m, j+\beta m, k+\gamma m}, \forall i, j, k, \alpha, \beta, \gamma \in \mathbb{Z} \right\}. \end{aligned}$$

The spaces $\mathcal{E}_{\text{per}}^y$ and $\mathcal{E}_{\text{per}}^z$ are analogously defined. The functions of \mathcal{C}_{per} are called *cell centered functions*. The functions of $\mathcal{E}_{\text{per}}^x$, $\mathcal{E}_{\text{per}}^y$, and $\mathcal{E}_{\text{per}}^z$, are called *east-west face-centered functions*, *north-south face-centered functions*, and *up-down face-centered functions*, respectively. We also define the mean zero space

$$\mathring{\mathcal{C}}_{\text{per}} := \left\{ \nu \in \mathcal{C}_{\text{per}} \mid \bar{\nu} := \frac{h^3}{|\Omega|} \sum_{i,j,k=1}^m \nu_{i,j,k} = 0 \right\}.$$

We now introduce the important difference and average operators on the spaces:

$$A_x \nu_{i+\frac{1}{2}, j, k} := \frac{1}{2} (\nu_{i+1, j, k} + \nu_{i, j, k}), \quad D_x \nu_{i+\frac{1}{2}, j, k} := \frac{1}{h} (\nu_{i+1, j, k} - \nu_{i, j, k}),$$

$$\begin{aligned} A_y \nu_{i,j+\frac{1}{2},k} &:= \frac{1}{2} (\nu_{i,j+1,k} + \nu_{i,j,k}), & D_y \nu_{i,j+\frac{1}{2},k} &:= \frac{1}{h} (\nu_{i,j+1,k} - \nu_{i,j,k}), \\ A_z \nu_{i,j,k+\frac{1}{2}} &:= \frac{1}{2} (\nu_{i,j,k+1} + \nu_{i,j,k}), & D_z \nu_{i,j,k+\frac{1}{2}} &:= \frac{1}{h} (\nu_{i,j,k+1} - \nu_{i,j,k}), \end{aligned}$$

with $A_x, D_x : \mathcal{C}_{\text{per}} \rightarrow \mathcal{E}_{\text{per}}^x$, $A_y, D_y : \mathcal{C}_{\text{per}} \rightarrow \mathcal{E}_{\text{per}}^y$, $A_z, D_z : \mathcal{C}_{\text{per}} \rightarrow \mathcal{E}_{\text{per}}^z$. Likewise,

$$\begin{aligned} a_x \nu_{i,j,k} &:= \frac{1}{2} (\nu_{i+\frac{1}{2},j,k} + \nu_{i-\frac{1}{2},j,k}), & d_x \nu_{i,j,k} &:= \frac{1}{h} (\nu_{i+\frac{1}{2},j,k} - \nu_{i-\frac{1}{2},j,k}), \\ a_y \nu_{i,j,k} &:= \frac{1}{2} (\nu_{i,j+\frac{1}{2},k} + \nu_{i,j-\frac{1}{2},k}), & d_y \nu_{i,j,k} &:= \frac{1}{h} (\nu_{i,j+\frac{1}{2},k} - \nu_{i,j-\frac{1}{2},k}), \\ a_z \nu_{i,j,k} &:= \frac{1}{2} (\nu_{i,j,k+\frac{1}{2}} + \nu_{i,j,k-\frac{1}{2}}), & d_z \nu_{i,j,k} &:= \frac{1}{h} (\nu_{i,j,k+\frac{1}{2}} - \nu_{i,j,k-\frac{1}{2}}), \end{aligned}$$

with $a_x, d_x : \mathcal{E}_{\text{per}}^x \rightarrow \mathcal{C}_{\text{per}}$, $a_y, d_y : \mathcal{E}_{\text{per}}^y \rightarrow \mathcal{C}_{\text{per}}$, and $a_z, d_z : \mathcal{E}_{\text{per}}^z \rightarrow \mathcal{C}_{\text{per}}$. The standard 3D discrete Laplacian, $\Delta_h : \mathcal{C}_{\text{per}} \rightarrow \mathcal{C}_{\text{per}}$, is given by

$$\begin{aligned} \Delta_h \nu_{i,j,k} &:= d_x(D_x \nu)_{i,j,k} + d_y(D_y \nu)_{i,j,k} + d_z(D_z \nu)_{i,j,k} \\ &= \frac{1}{h^2} (\nu_{i+1,j,k} + \nu_{i-1,j,k} + \nu_{i,j+1,k} + \nu_{i,j-1,k} + \nu_{i,j,k+1} + \nu_{i,j,k-1} - 6\nu_{i,j,k}). \end{aligned}$$

Now we are ready to define the following grid inner products:

$$\begin{aligned} (\nu, \xi)_2 &:= h^3 \sum_{i,j,k=1}^m \nu_{i,j,k} \xi_{i,j,k}, & \nu, \xi &\in \mathcal{C}_{\text{per}}, & [\nu, \xi]_x &:= (a_x(\nu \xi), 1)_2, & \nu, \xi &\in \mathcal{E}_{\text{per}}^x, \\ [\nu, \xi]_y &:= (a_y(\nu \xi), 1)_2, & \nu, \xi &\in \mathcal{E}_{\text{per}}^y, & [\nu, \xi]_z &:= (a_z(\nu \xi), 1)_2, & \nu, \xi &\in \mathcal{E}_{\text{per}}^z. \end{aligned}$$

We now define the following norms for cell-centered functions. If $\nu \in \mathcal{C}_{\text{per}}$, then $\|\nu\|_2^2 := (\nu, \nu)_2$; $\|\nu\|_p^p := (|\nu|^p, 1)_2$ ($1 \leq p < \infty$), and $\|\nu\|_\infty := \max_{1 \leq i,j,k \leq m} |\nu_{i,j,k}|$. Similarly, we define the gradient norms: for $\nu \in \mathcal{C}_{\text{per}}$,

$$\|\nabla_h \nu\|_2^2 := [D_x \nu, D_x \nu]_x + [D_y \nu, D_y \nu]_y + [D_z \nu, D_z \nu]_z.$$

Consequently,

$$\|\nu\|_{2,2}^2 := \|\nu\|_2^2 + \|\nabla_h \nu\|_2^2 + \|\Delta_h \nu\|_2^2.$$

In addition, the discrete energy $F_h(\phi) : \mathcal{C}_{\text{per}} \rightarrow \mathbb{R}$ is defined as

$$F_h(\phi) = \frac{1}{4} \|\phi\|_4^4 + \frac{1-\epsilon}{2} \|\phi\|_2^2 - \|\nabla_h \phi\|_2^2 + \frac{1}{2} \|\Delta_h \phi\|_2^2. \quad (2.1)$$

The following preliminary estimates are cited from earlier works. For more details we refer the reader to [46, 69].

Lemma 2.1. *For any $f, g \in \mathcal{C}_{\text{per}}$, the following summation by parts formulas are valid:*

$$(f, \Delta_h g) = -(\nabla_h f, \nabla_h g), \quad (f, \Delta_h^2 g) = (\Delta_h f, \Delta_h g), \quad (f, \Delta_h^3 g) = -(\nabla_h \Delta_h f, \nabla_h \Delta_h g). \quad (2.2)$$

Lemma 2.2. *Suppose $\phi \in \mathcal{C}_{\text{per}}$. Then*

$$\|\Delta_h \phi\|_2^2 \leq \frac{1}{3\alpha^2} \|\phi\|_2^2 + \frac{2\alpha}{3} \|\nabla_h(\Delta_h \phi)\|_2^2, \quad (2.3)$$

is valid for arbitrary $\alpha > 0$.

Lemma 2.3. For $\phi \in \mathcal{C}_{\text{per}}$, we have the estimate

$$F_h(\phi) \geq C\|\phi\|_{2,2}^2 - \frac{L^3}{4}, \quad (2.4)$$

with C only dependent on Ω , and $F_h(\phi)$ given by (2.1).

3 The fully discrete second order numerical scheme and the main results

Let $N_t \in \mathbb{Z}^+$, and set $\tau := T/N_t$, where T is the final time. For our present and future use, we define the canonical grid projection operator $P_h : C^0(\Omega) \rightarrow \mathcal{C}_{\text{per}}$ via $[P_h v]_{i,j,k} = v(\xi_i, \xi_j, \xi_k)$. Set $u_{h,s} := P_h u(\cdot, s)$. Then $F_h(u_{h,0}, u_{h,s}) + \frac{1}{2}\|\nabla_h(u_{h,s} - u_{h,0})\|_2^2 \rightarrow F_h(u(\cdot, 0))$ as $h \rightarrow 0$ and $s \rightarrow 0$ for sufficiently regular u . We denote ϕ_e as the exact solution to the PFC equation (1.2) and take $\Phi_{i,j,k}^\ell = P_h \phi_e(\cdot, t_\ell)$.

Our second order numerical scheme in [46] can be formulated as follows: for $1 \leq \kappa \leq N_t$, given $\phi^\kappa, \phi^{\kappa-1} \in \mathcal{C}_{\text{per}}$, find $\phi^{\kappa+1}, \mu^{\kappa+\frac{1}{2}}, \omega^{\kappa+\frac{1}{2}} \in \mathcal{C}_{\text{per}}$ periodic such that

$$\begin{aligned} \frac{\phi^{\kappa+1} - \phi^\kappa}{\tau} &= \Delta_h \mu^{\kappa+\frac{1}{2}}, \\ \mu^{\kappa+\frac{1}{2}} &:= (\phi^{\kappa+\frac{1}{2}})(\phi^2)^{\kappa+\frac{1}{2}} + (1-\epsilon)\phi^{\kappa+\frac{1}{2}} + 3\Delta_h \phi^\kappa - \Delta_h \phi^{\kappa-1} + \Delta_h \omega^{\kappa+\frac{1}{2}}, \\ \omega^{\kappa+\frac{1}{2}} &:= \Delta_h \phi^{\kappa+1}, \end{aligned} \quad (3.1)$$

where $\phi^0 := \Phi^0$, $\phi^1 := \Phi^1$.

The unique solvability and energy stability have already been established in [46]; see the following result.

Proposition 3.1. [46] Suppose that the initial profiles $\phi^0, \phi^1 \in \mathcal{C}_{\text{per}}$ satisfy periodic boundary condition, with sufficient regularity assumption for the exact solution ϕ_e . Given any $(\phi^{m-1}, \phi^m) \in \mathcal{C}_{\text{per}}$, there is a unique solution $\phi^{m+1} \in \mathcal{C}_{\text{per}}$ to the scheme (3.1). The scheme (3.1), with starting values ϕ^0 and ϕ^1 , is unconditionally energy stable, i.e., for any $\tau > 0$ and $h > 0$, and any positive integer $1 \leq \kappa \leq N_t$,

$$F_h(\phi^\kappa) \leq F_h(\phi^1) + \frac{1}{2}\|\nabla_h(\phi^1 - \phi^0)\|_2^2 \leq C_0, \quad (3.2)$$

in which C_0 is independent on h , τ , ϵ and T .

The $\|\cdot\|_\infty$ bound of a grid function could be controlled with the help of a discrete Sobolev inequality, as stated by the following theorem; its proof will be given in Section 4.

Theorem 3.2. Let $\phi \in \mathcal{C}_{\text{per}}$. Then there exists a constant C independent of τ or h such that

$$\|\phi\|_\infty \leq C\|\phi\|_{2,2}. \quad (3.3)$$

As a combination of Proposition 3.1, Theorem 3.2 and inequality (2.4) in Lemma 2.3, the following $\|\cdot\|_\infty$ estimate for the numerical solution is available.

Corollary 3.3. *For the numerical scheme (3.1), we have*

$$\|\phi^\kappa\|_\infty \leq C \left(C_0 + \frac{L^3}{4} \right) := \tilde{C}_0, \quad \forall \kappa \geq 0. \quad (3.4)$$

The main theoretical result is stated in the following theorem; Its proof will be given in Section 4.

Theorem 3.4. *Suppose the unique solution ϕ_e for the three-dimensional PFC equation (1.2), with $M(\phi) \equiv 1$, is of regularity class*

$$\phi_e \in \mathcal{R} := H^3(0, T; C_{\text{per}}^0) \cap H^2(0, T; C_{\text{per}}^4) \cap L^\infty(0, T; C_{\text{per}}^8), \quad (3.5)$$

and the initial data $\phi^0, \phi^1 \in \mathcal{C}_{\text{per}}$ are defined as above. Define $e_{ijk}^\kappa := \Phi_{ijk}^\kappa - \phi_{ijk}^\kappa$. Then, provided τ and h are sufficiently small, for all positive integers κ , such that $\tau \cdot \kappa \leq T$, we have

$$\|e^\kappa\|_2 \leq C(h^2 + \tau^2), \quad (3.6)$$

for some $C > 0$ that is independent of h and τ .

4 The detailed convergence analysis

4.1 The proof of Theorem 3.2

We begin with the proof of Theorem 3.2, which provides a tool to bound the $\|\cdot\|_\infty$ norm of a grid function in terms of its discrete $\|\cdot\|_{2,2}$ norm.

Proof. For a function $\phi \in \mathcal{C}_{\text{per}}$ with value ϕ_{ijk} at (x_i, y_j, z_k) , the IDFT is given by [61]:

$$\phi_{ijk} = \sum_{r,s,t=-R}^R \hat{\phi}_{rst} e^{2\pi i(rx_i + sy_j + tz_k)/L}, \quad i, j, k = 1, \dots, m, \quad (4.1)$$

in which $m = 2R + 1$. In turn, the corresponding interpolation function is defined as

$$\phi_F(x, y, z) = \sum_{r,s,t=-R}^R \hat{\phi}_{rst} e^{2\pi i(rx + sy + tz)/L}.$$

Using the Parseval's identity (at both the discrete and continuous levels), we have

$$\|\phi\|_2^2 = \|\phi_F\|_{L^2}^2 = L^3 \sum_{r,s,t=-R}^R |\hat{\phi}_{rst}|^2,$$

$$\begin{aligned} D_x \phi_{i+\frac{1}{2},j,k} &= \frac{1}{h} (\phi_{i+1,j,k} - \phi_{i,j,k}) \\ &= \frac{1}{h} \sum_{r,s,t=-R}^R \hat{\phi}_{rst} \left[e^{2\pi i(rx_{i+1} + sy_j + tz_k)/L} - e^{2\pi i(rx_i + sy_j + tz_k)/L} \right] \\ &= \frac{1}{h} \sum_{r,s,t=-R}^R \hat{\phi}_{rst} e^{2\pi i(rx_{i+\frac{1}{2}} + sy_j + tz_k)/L} \cdot 2i \sin \frac{\pi r h}{L} \\ &= \sum_{r,s,t=-R}^R u_r \hat{\phi}_{rst} e^{2\pi i(rx_{i+\frac{1}{2}} + sy_j + tz_k)/L}, \end{aligned}$$

$$\partial_x \phi_F(x, y, z) = \sum_{r,s,t=-R}^R v_r \hat{\phi}_{rst} e^{2\pi i(rx+sy+tz)/L},$$

with

$$u_r = \frac{2i \sin \frac{\pi r h}{L}}{h}, \quad v_r = \frac{2i \pi r}{L}.$$

A comparison of Fourier eigenvalues between $|u_r|$ and $|v_r|$ shows that

$$\frac{2}{\pi} |v_r| \leq |u_r| \leq |v_r|, \quad -R \leq r \leq R,$$

$$[D_x \phi, D_x \phi]_x = h^3 \sum_{i,j,k=1}^m |D_x \phi_{i+\frac{1}{2},j,k}|^2 = L^3 \sum_{r,s,t=-R}^R |u_r|^2 |\hat{\phi}_{rst}|^2,$$

$$\|\partial_x \phi_F\|^2 = L^3 \sum_{r,s,t=-R}^R |v_r|^2 |\hat{\phi}_{rst}|^2.$$

Then we get

$$\|\partial_x \phi_F\|^2 = \left| \frac{v_r}{u_r} \right|^2 [D_x \phi, D_x \phi]_x \leq \left(\frac{\pi}{2} \right)^2 [D_x \phi, D_x \phi]_x,$$

Similarly, the following estimates are available:

$$\|\partial_y \phi_F\|^2 \leq \left(\frac{\pi}{2} \right)^2 [D_y \phi, D_y \phi]_y,$$

$$\|\partial_z \phi_F\|^2 \leq \left(\frac{\pi}{2} \right)^2 [D_z \phi, D_z \phi]_z.$$

For the second order derivatives, the following estimates are valid:

$$\begin{aligned} & d_x(D_x \phi)_{i,j,k} \\ &= \frac{1}{h} (D_x \phi_{i+\frac{1}{2},j,k} - D_x \phi_{i-\frac{1}{2},j,k}) \\ &= \frac{1}{h} \left(\sum_{r,s,t=-R}^R u_r \hat{\phi}_{rst} e^{2\pi i(rx_{i+\frac{1}{2}}+sy_j+tz_k)/L} - \sum_{r,s,t=-R}^R u_r \hat{\phi}_{rst} e^{2\pi i(rx_{i-\frac{1}{2}}+sy_j+tz_k)/L} \right) \\ &= \sum_{r,s,t=-R}^R u_r^2 \hat{\phi}_{rst} e^{2\pi i(rx_i+sy_j+tz_k)/L}, \end{aligned}$$

$$\partial_x^2 \phi_F(x, y, z) = \sum_{r,s,t=-R}^R v_r^2 \hat{\phi}_{rst} e^{2\pi i(rx+sy+tz)/L}.$$

As a consequence, these inequalities yield the following result:

$$\|\partial_x^2 \phi_F\|^2 = \left| \frac{v_r}{u_r} \right|^4 \|d_x(D_x \phi)\|_2^2 \leq \left(\frac{\pi}{2} \right)^4 \|d_x(D_x \phi)\|_2^2.$$

Similarly,

$$\|\partial_y^2 \phi_F\|^2 \leq \left(\frac{\pi}{2} \right)^4 \|d_y(D_y \phi)\|_2^2, \quad \|\partial_z^2 \phi_F\|^2 \leq \left(\frac{\pi}{2} \right)^4 \|d_z(D_z \phi)\|_2^2,$$

and

$$\begin{aligned}\|\partial_x \partial_y \phi_F\|^2 &\leq \frac{1}{2}(\|\partial_x^2 \phi_F\|^2 + \|\partial_y^2 \phi_F\|^2), \\ \|\partial_x \partial_z \phi_F\|^2 &\leq \frac{1}{2}(\|\partial_x^2 \phi_F\|^2 + \|\partial_z^2 \phi_F\|^2), \\ \|\partial_y \partial_z \phi_F\|^2 &\leq \frac{1}{2}(\|\partial_y^2 \phi_F\|^2 + \|\partial_z^2 \phi_F\|^2).\end{aligned}$$

Then we arrive at

$$\begin{aligned}\|\phi_F\|_{H^2}^2 &= |\phi_F|_{0,2}^2 + |\phi_F|_{1,2}^2 + |\phi_F|_{2,2}^2 \\ &\leq \|\phi_F\|^2 + \|\partial_x \phi_F\|^2 + \|\partial_y \phi_F\|^2 + \|\partial_z \phi_F\|^2 + 2(\|\partial_x^2 \phi_F\|^2 + \|\partial_y^2 \phi_F\|^2 + \|\partial_z^2 \phi_F\|^2) \\ &\leq \|\phi\|_2^2 + \left(\frac{\pi}{2}\right)^2 ([D_x \phi, D_x \phi]_x + [D_y \phi, D_y \phi]_y + [D_z \phi, D_z \phi]_z) \\ &\quad + 2 \times \left(\frac{\pi}{2}\right)^4 (\|d_x(D_x \phi)\|_2^2 + \|d_y(D_y \phi)\|_2^2 + \|d_z(D_z \phi)\|_2^2) \\ &= \|\phi\|_2^2 + \left(\frac{\pi}{2}\right)^2 \|\nabla_h \phi\|_2^2 + 2 \times \left(\frac{\pi}{2}\right)^4 \|\Delta_h \phi\|_2^2 \\ &\leq 2 \cdot \left(\frac{\pi}{2}\right)^4 (\|\phi\|_2^2 + \|\nabla_h \phi\|_2^2 + \|\Delta_h \phi\|_2^2) \\ &= 2 \cdot \left(\frac{\pi}{2}\right)^4 \|\phi\|_{2,2}^2.\end{aligned}$$

Meanwhile, since ϕ is the discrete interpolate of the continuous function, an obvious observation that $\|\phi\|_\infty \leq \|\phi_F\|_{L^\infty}$ implies the following estimate:

$$\|\phi\|_\infty \leq \|\phi_F\|_{L^\infty} \leq C_1 \|\phi_F\|_{H^2} \leq \frac{\sqrt{2}\pi^2}{4} C_1 \|\phi\|_{2,2},$$

which gives (3.3). This completes the proof of Theorem 3.2.

4.2 The proof of Theorem 3.4

Corollary 3.3 is a direct consequence of Theorem 3.2, so that a uniform in time $\|\cdot\|_\infty$ bound of the numerical solution becomes available. With the help of the bound (3.4), we proceed into the convergence proof in Theorem 3.4.

Proof. An application of the Taylor expansion for the exact solution Φ at $(x_i, y_j, z_k, t_{\kappa+\frac{1}{2}})$ implies that

$$\begin{aligned}\frac{\Phi_{ijk}^{\kappa+1} - \Phi_{ijk}^\kappa}{\tau} &= \Delta_h U_{ijk}^{\kappa+\frac{1}{2}} + R_{ijk}^\kappa, \quad 1 \leq i \leq m, \quad 1 \leq j \leq n, \quad 1 \leq k \leq l, \quad 1 \leq s \leq N_t, \\ U_{ijk}^{\kappa+\frac{1}{2}} &= (\Phi_{ijk}^{\kappa+\frac{1}{2}})(\Phi_{ijk}^2)^{\kappa+\frac{1}{2}} + (1-\epsilon)\Phi_{ijk}^{\kappa+\frac{1}{2}} + 3\Delta_h \Phi_{ijk}^\kappa - \Delta_h \Phi_{ijk}^{\kappa-1} + \Delta_h(\Delta_h \Phi_{ijk})^{\kappa+\frac{1}{2}} + S_{ijk}^\kappa, \quad (4.2) \\ &\quad 1 \leq i \leq m, \quad 1 \leq j \leq n, \quad 1 \leq k \leq l, \quad 1 \leq \kappa \leq N_t, \\ \Phi_{ijk}^0 &= \psi(x_i, y_j, z_k) \quad 1 \leq i \leq m, \quad 1 \leq j \leq n, \quad 1 \leq k \leq l,\end{aligned}$$

in which the local truncation errors R_{ijk}^κ and S_{ijk}^κ satisfy

$$|R_{ijk}^\kappa| \leq C_3(\tau^2 + h^2), \quad |S_{ijk}^\kappa| \leq C_3(\tau^2 + h^2), \quad 1 \leq i \leq m, \quad 1 \leq j \leq n, \quad 1 \leq k \leq l, \quad 1 \leq \kappa \leq N_t, \quad (4.3)$$

for some $C_3 \geq 0$, dependent only on T and L .

To facilitate the convergence analysis, we denote

$$C_4 = \|\Phi\|_{L^\infty(0,T;\Omega)}. \quad (4.4)$$

The uniform in time $\|\cdot\|_\infty$ bound for the numerical solution is given by \tilde{C}_0 , as defined as (3.4). These two bounds will be useful in the nonlinear error estimate.

Subtracting (3.1) from (4.2) leads to the following error evolutionary equation:

$$\begin{aligned} \frac{e^{\kappa+1} - e^\kappa}{\tau} = \Delta_h \left\{ \left[(\Phi^{\kappa+\frac{1}{2}})(\Phi^2)^{\kappa+\frac{1}{2}} - (\phi^{\kappa+\frac{1}{2}})(\phi^2)^{\kappa+\frac{1}{2}} \right] + (1-\epsilon)e^{\kappa+\frac{1}{2}} \right. \\ \left. + (3\Delta_h e^\kappa - \Delta_h e^{\kappa-1}) + \Delta_h(\Delta_h e)^{\kappa+\frac{1}{2}} + S^\kappa \right\} + R^\kappa. \end{aligned} \quad (4.5)$$

Taking a discrete inner product with (4.5) by $e^{\kappa+\frac{1}{2}}$, we get

$$\begin{aligned} \left(\frac{e^{\kappa+1} - e^\kappa}{\tau}, e^{\kappa+\frac{1}{2}} \right) = \left(\Phi^{\kappa+\frac{1}{2}}(\Phi^2)^{\kappa+\frac{1}{2}} - \phi^{\kappa+\frac{1}{2}}(\phi^2)^{\kappa+\frac{1}{2}}, \Delta_h e^{\kappa+\frac{1}{2}} \right) + (1-\epsilon)(\Delta_h e^{\kappa+\frac{1}{2}}, e^{\kappa+\frac{1}{2}}) \\ + \left(\Delta_h(3\Delta_h e^\kappa - \Delta_h e^{\kappa-1}), e^{\kappa+\frac{1}{2}} \right) + \left(\Delta_h^3 e^{\kappa+\frac{1}{2}}, e^{\kappa+\frac{1}{2}} \right) \\ + (\Delta_h S^\kappa, e^{\kappa+\frac{1}{2}}) + (R^\kappa, e^{\kappa+\frac{1}{2}}). \end{aligned} \quad (4.6)$$

For the left hand side of (4.6), the following identity is valid:

$$\left(\frac{e^{\kappa+1} - e^\kappa}{\tau}, e^{\kappa+\frac{1}{2}} \right) = \frac{1}{2\tau} (\|e^{\kappa+1}\|_2^2 - \|e^\kappa\|_2^2). \quad (4.7)$$

For the nonlinear error term on the right hand side of (4.6), we have

$$\begin{aligned} & \left(\Phi^{\kappa+\frac{1}{2}}(\Phi^2)^{\kappa+\frac{1}{2}} - \phi^{\kappa+\frac{1}{2}}(\phi^2)^{\kappa+\frac{1}{2}}, \Delta_h e^{\kappa+\frac{1}{2}} \right) \\ &= \left(\Phi^{\kappa+\frac{1}{2}} \frac{(\Phi^\kappa)^2 + (\Phi^{\kappa+1})^2}{2} - \phi^{\kappa+\frac{1}{2}} \frac{(\phi^\kappa)^2 + (\phi^{\kappa+1})^2}{2}, \Delta_h e^{\kappa+\frac{1}{2}} \right) \\ &= \left(\Phi^{\kappa+\frac{1}{2}} \left(\frac{(\Phi^{\kappa+1})^2 - (\phi^{\kappa+1})^2}{2} + \frac{(\Phi^\kappa)^2 - (\phi^\kappa)^2}{2} \right) + (\Phi^{\kappa+\frac{1}{2}} - \phi^{\kappa+\frac{1}{2}}) \frac{(\phi^\kappa)^2 + (\phi^{\kappa+1})^2}{2}, \Delta_h e^{\kappa+\frac{1}{2}} \right) \\ &= \left(\Phi^{\kappa+\frac{1}{2}} \left(\frac{\Phi^{\kappa+1} + \phi^{\kappa+1}}{2} e^{\kappa+1} + \frac{\Phi^\kappa + \phi^\kappa}{2} e^\kappa \right) + \frac{(\phi^\kappa)^2 + (\phi^{\kappa+1})^2}{2} e^{\kappa+\frac{1}{2}}, \Delta_h e^{\kappa+\frac{1}{2}} \right) \\ &\leq \frac{1}{4} \left[2C_4^2 + (C_4 + \tilde{C}_0)^2 \right] (\|e^{\kappa+1}\|_2 + \|e^\kappa\|_2) \cdot \|\Delta_h e^{\kappa+\frac{1}{2}}\|_2 \\ &\leq \frac{1}{2} \|\Delta_h e^{\kappa+\frac{1}{2}}\|_2^2 + C(C_4^4 + \tilde{C}_0^4) (\|e^{\kappa+1}\|_2^2 + \|e^\kappa\|_2^2), \end{aligned} \quad (4.8)$$

in which the discrete Hölder inequality has been repeatedly applied. The second and fourth terms on the right hand side of (4.6) could be analyzed in a straightforward way:

$$(1-\epsilon)(\Delta_h e^{\kappa+\frac{1}{2}}, e^{\kappa+\frac{1}{2}}) = -(1-\epsilon)\|\nabla_h e^{\kappa+\frac{1}{2}}\|_2^2, \quad (4.9)$$

$$\left(\Delta_h^3 e^{\kappa+\frac{1}{2}}, e^{\kappa+\frac{1}{2}} \right) = -\|\nabla_h \Delta_h e^{\kappa+\frac{1}{2}}\|_2^2. \quad (4.10)$$

For the third term of the right hand side of (4.6), the following estimate is applied:

$$\left(\Delta_h(3\Delta_h e^\kappa - \Delta_h e^{\kappa-1}), e^{\kappa+\frac{1}{2}} \right) \quad (4.11)$$

$$= (3\Delta_h e^\kappa - \Delta_h e^{\kappa-1}, \Delta_h e^{\kappa+\frac{1}{2}}) = (3\Delta_h e^\kappa - \Delta_h (2e^{\kappa-\frac{1}{2}} - e^\kappa), \Delta_h e^{\kappa+\frac{1}{2}}) \quad (4.12)$$

$$= (4\Delta_h e^\kappa - 2\Delta_h e^{\kappa-\frac{1}{2}}, \Delta_h e^{\kappa+\frac{1}{2}}) \quad (4.13)$$

$$= ((2\Delta_h e^{\kappa+1} + 2\Delta_h e^\kappa) - (2\Delta_h e^{\kappa+1} - 2\Delta_h e^\kappa) - 2\Delta_h e^{\kappa-\frac{1}{2}}, \Delta_h e^{\kappa+\frac{1}{2}}) \quad (4.14)$$

$$= 4\|\Delta_h e^{\kappa+\frac{1}{2}}\|_2^2 - \|\Delta_h e^{\kappa+1}\|_2^2 + \|\Delta_h e^\kappa\|_2^2 - 2(\Delta_h e^{\kappa-\frac{1}{2}}, \Delta_h e^{\kappa+\frac{1}{2}}) \quad (4.15)$$

$$\leq 4\|\Delta_h e^{\kappa+\frac{1}{2}}\|_2^2 - \|\Delta_h e^{\kappa+1}\|_2^2 + \|\Delta_h e^\kappa\|_2^2 + \|\Delta_h e^{\kappa-\frac{1}{2}}\|_2^2 + \|\Delta_h e^{\kappa+\frac{1}{2}}\|_2^2 \quad (4.16)$$

$$\leq 5\|\Delta_h e^{\kappa+\frac{1}{2}}\|_2^2 + \|\Delta_h e^{\kappa-\frac{1}{2}}\|_2^2 - \|\Delta_h e^{\kappa+1}\|_2^2 + \|\Delta_h e^\kappa\|_2^2. \quad (4.17)$$

The fifth term and sixth terms on the right hand side of (4.6) could be bounded with an application of Cauchy inequality:

$$(\Delta_h S^\kappa, e^{\kappa+\frac{1}{2}}) \leq \frac{1}{2}\|S^\kappa\|_2^2 + \frac{1}{2}\|\Delta_h e^{\kappa+\frac{1}{2}}\|_2^2, \quad (4.18)$$

$$(R^\kappa, e^{\kappa+\frac{1}{2}}) \leq \frac{1}{2}\|R^\kappa\|_2^2 + \frac{1}{2}\|e^{\kappa+\frac{1}{2}}\|_2^2. \quad (4.19)$$

Therefore, a substitution of (4.7)-(4.18) into (4.6) yields

$$\begin{aligned} & \frac{1}{2\tau}(\|e^{\kappa+1}\|_2^2 - \|e^\kappa\|_2^2) + \|\nabla_h \Delta_h e^{\kappa+\frac{1}{2}}\|_2^2 + (1-\epsilon)\|\nabla_h e^{\kappa+\frac{1}{2}}\|_2^2 \\ & \leq C(C_4^4 + \tilde{C}_0^4)(\|e^{\kappa+1}\|_2^2 + \|e^\kappa\|_2^2) + \frac{1}{2}\|e^{\kappa+\frac{1}{2}}\|_2^2 + \frac{1}{2}(\|S^\kappa\|_2^2 + \|R^\kappa\|_2^2) \\ & \quad + 6\|\Delta_h e^{\kappa+\frac{1}{2}}\|_2^2 + \|\Delta_h e^{\kappa-\frac{1}{2}}\|_2^2 - \|\Delta_h e^{\kappa+1}\|_2^2 + \|\Delta_h e^\kappa\|_2^2 \\ & \leq C(C_4^4 + \tilde{C}_0^4 + 1)(\|e^{\kappa+1}\|_2^2 + \|e^\kappa\|_2^2) + \frac{1}{2}(\|S^\kappa\|_2^2 + \|R^\kappa\|_2^2) \\ & \quad + 6\|\Delta_h e^{\kappa+\frac{1}{2}}\|_2^2 + \|\Delta_h e^{\kappa-\frac{1}{2}}\|_2^2 - \|\Delta_h e^{\kappa+1}\|_2^2 + \|\Delta_h e^\kappa\|_2^2. \end{aligned} \quad (4.20)$$

By Lemma 2.2, we obtain

$$6\|\Delta_h e^{\kappa+\frac{1}{2}}\|_2^2 \leq 6\left(\frac{12^2}{3}\|e^{\kappa+\frac{1}{2}}\|_2^2 + \frac{2}{36}\|\nabla_h \Delta_h e^{\kappa+\frac{1}{2}}\|_2^2\right), \quad (4.21)$$

$$\|\Delta_h e^{\kappa-\frac{1}{2}}\|_2^2 \leq \left(\frac{1^2}{3}\|e^{\kappa-\frac{1}{2}}\|_2^2 + \frac{2}{3}\|\nabla_h \Delta_h e^{\kappa-\frac{1}{2}}\|_2^2\right). \quad (4.22)$$

Going back (4.20), we arrive at

$$\begin{aligned} & \frac{1}{2\tau}(\|e^{\kappa+1}\|_2^2 - \|e^\kappa\|_2^2) + \|\nabla_h \Delta_h e^{\kappa+\frac{1}{2}}\|_2^2 + \|\Delta_h e^{\kappa+1}\|_2^2 - \|\Delta_h e^\kappa\|_2^2 \\ & \leq 288\|e^{\kappa+\frac{1}{2}}\|_2^2 + \frac{1}{3}\|\nabla_h \Delta_h e^{\kappa+\frac{1}{2}}\|_2^2 + \frac{1}{3}\|e^{\kappa-\frac{1}{2}}\|_2^2 + \frac{2}{3}\|\nabla_h \Delta_h e^{\kappa-\frac{1}{2}}\|_2^2 \\ & \quad + \frac{1}{2}(\|S^\kappa\|_2^2 + \|R^\kappa\|_2^2) + C(C_4^4 + \tilde{C}_0^4 + 1)(\|e^{\kappa+1}\|_2^2 + \|e^\kappa\|_2^2). \end{aligned} \quad (4.23)$$

A summation in time implies that

$$\begin{aligned} & \frac{1}{2\tau}(\|e^{\kappa+1}\|_2^2 - \|e^0\|_2^2) + \|\Delta_h e^{\kappa+1}\|_2^2 - \|\Delta_h e^0\|_2^2 \\ & \leq \frac{1}{2} \sum_{i=0}^{\kappa} (\|S^i\|_2^2 + \|R^i\|_2^2) + C \sum_{i=0}^{\kappa} (C_4^4 + \tilde{C}_0^4 + 1)(\|e^{i+1}\|_2^2 + \|e^i\|_2^2 + \|e^{i-1}\|_2^2). \end{aligned} \quad (4.24)$$

In turn, an application of discrete Gronwall inequality yields the desired convergence result (3.6). This completes the proof of Theorem 3.4.

5 Nonlinear multigrid solvers

In this section we present the details of the nonlinear multigrid method that we use for solving the semi-implicit numerical scheme (3.1). The fully finite-difference scheme (3.1) is formulated as follows: Find $\phi_{i,j,k}^{\kappa+1}$, $\mu_{i,j,k}^{\kappa+1/2}$ and $\kappa_{i,j,k}^{\kappa+1/2}$ in \mathcal{C}_{per} such that

$$\begin{aligned} & \phi_{i,j,k}^{\kappa+1} - \tau d_x \left(M \left(A_x \phi_*^{\kappa+1/2} \right) D_x \mu^{\kappa+1/2} \right)_{i,j,k} \\ & - \tau d_y \left(M \left(A_y \phi_*^{\kappa+1/2} \right) D_y \mu^{\kappa+1/2} \right)_{i,j,k} - \tau d_z \left(M \left(A_z \phi_*^{\kappa+1/2} \right) D_z \mu^{\kappa+1/2} \right)_{i,j,k} = \phi_{i,j,k}^{\kappa}, \end{aligned} \quad (5.1)$$

$$\begin{aligned} & \mu_{i,j,k}^{\kappa+1/2} - \frac{1}{4} \left(\phi_{i,j,k}^{\kappa+1} + \phi_{i,j,k}^{\kappa} \right) \left((\phi_{i,j,k}^{\kappa+1})^2 + (\phi_{i,j,k}^{\kappa})^2 \right) - \frac{1-\epsilon}{2} \left(\phi_{i,j,k}^{\kappa+1} + \phi_{i,j,k}^{\kappa} \right) \\ & - 3\Delta_h \phi_{i,j,k}^{\kappa} + \Delta_h \phi_{i,j,k}^{\kappa-1} - \Delta_h \omega_{i,j,k}^{\kappa+1} = 0, \end{aligned} \quad (5.2)$$

$$\omega_{i,j,k}^{\kappa+1/2} - \frac{1}{2} \left(\Delta_h \phi_{i,j,k}^{\kappa+1} + \Delta_h \phi_{i,j,k}^{\kappa} \right) = 0, \quad (5.3)$$

where $\phi_*^{\kappa+1/2} = \frac{3}{2}\phi^{\kappa} - \frac{1}{2}\phi^{\kappa-1}$. Denote $\mathbf{u} = (\phi_{i,j,k}^{\kappa+1}, \mu_{i,j,k}^{\kappa+1/2}, \omega_{i,j,k}^{\kappa+1/2})^T$. Then the above discrete nonlinear system can be written in terms of a nonlinear operator \mathbf{N} and source term \mathbf{S} such that

$$\mathbf{N}(\mathbf{u}) = \mathbf{S}. \quad (5.4)$$

The $3 \times m \times n \times l$ nonlinear operator $\mathbf{N}(\mathbf{u}^{\kappa+1}) = (N_{i,j,k}^{(1)}(\mathbf{u}), N_{i,j,k}^{(2)}(\mathbf{u}), N_{i,j,k}^{(3)}(\mathbf{u}))^T$ can be defined as

$$\begin{aligned} N_{i,j,k}^{(1)}(\mathbf{u}) &= \phi_{i,j,k}^{\kappa+1} - \tau d_x \left(M \left(A_x \phi_*^{\kappa+1/2} \right) D_x \mu^{\kappa+1/2} \right)_{i,j,k} - \tau d_y \left(M \left(A_y \phi_*^{\kappa+1/2} \right) D_y \mu^{\kappa+1/2} \right)_{i,j,k} \\ & - \tau d_z \left(M \left(A_z \phi_*^{\kappa+1/2} \right) D_z \mu^{\kappa+1/2} \right)_{i,j,k}, \end{aligned} \quad (5.5)$$

$$N_{i,j,k}^{(2)}(\mathbf{u}) = \mu_{i,j,k}^{\kappa+1/2} - \frac{1}{4} \left(\phi_{i,j,k}^{\kappa+1} + \phi_{i,j,k}^{\kappa} \right) \left((\phi_{i,j,k}^{\kappa+1})^2 + (\phi_{i,j,k}^{\kappa})^2 \right) - \frac{1-\epsilon}{2} \phi_{i,j,k}^{\kappa+1} - \Delta_h \omega_{i,j,k}^{\kappa+1}, \quad (5.6)$$

$$N_{i,j,k}^{(3)}(\mathbf{u}) = \omega_{i,j,k}^{\kappa+1/2} - \frac{1}{2} \Delta_h \phi_{i,j,k}^{\kappa+1}, \quad (5.7)$$

and the $3 \times m \times n \times l$ source $\mathbf{S} = (S_{i,j,k}^{(1)}, S_{i,j,k}^{(2)}, S_{i,j,k}^{(3)})^T$ is given by

$$S_{i,j,k}^{(1)} = \phi_{i,j,k}^{\kappa}, \quad (5.8)$$

$$S_{i,j,k}^{(2)} = \frac{1-\epsilon}{2} \phi_{i,j,k}^{\kappa} + 3\Delta_h \phi_{i,j,k}^{\kappa} - \Delta_h \phi_{i,j,k}^{\kappa-1}, \quad (5.9)$$

$$S_{i,j,k}^{(3)} = \frac{1}{2} \Delta_h \phi_{i,j,k}^{\kappa}. \quad (5.10)$$

The system (5.4) can be efficiently solved using a nonlinear Full Approximation Scheme (FAS) multigrid method (Algorithm 1: ν_1 and ν_2 are pre-smoothing and post-smoothing steps, ℓ, L are the current level and coarsest levels, and $\mathbf{I}_{\ell}^{\ell+1}, \mathbf{I}_{\ell+1}^{\ell}$ are coarsening and interpolating operators, respectively). More details can be found in [62]. Since we are using a standard FAS V-cycle approach, as reported in earlier works [8, 30, 46, 41, 68], we only provide the details of nonlinear smoothing scheme. For smoothing operator, we use a nonlinear Gauss-Seidel method with Red-Black ordering.

Algorithm 1 Nonlinear Multigrid Method (FAS)

```

1: Given  $\mathbf{u}^0$ 
2: procedure FAS( $\mathbf{N}^0, \mathbf{u}^0, \mathbf{S}^0, \nu_1, \nu_2, \ell = 0$ )
3:   while residual > tolerance do
4:     Pre-smooth:  $\mathbf{u}^\ell := \text{smooth}(\mathbf{N}^\ell, \mathbf{u}^\ell, \mathbf{S}^\ell, \nu_1)$  ▷ nonlinear Gauss-Seidel method
5:     Residual :  $\mathbf{r}^\ell = \mathbf{S}^\ell - \mathbf{N}^\ell \mathbf{u}^\ell$ 
6:     Coarsening:  $\mathbf{r}^{\ell+1} = \mathbf{I}_\ell^{\ell+1} \mathbf{r}^\ell, \mathbf{u}^{\ell+1} = \mathbf{I}_\ell^{\ell+1} \mathbf{u}^\ell$ 
7:     if  $\ell = L$  then
8:       Solve:  $\mathbf{N}^{\ell+1} \mathbf{v}^{\ell+1} = \mathbf{N}^{\ell+1} \mathbf{u}^{\ell+1} + \mathbf{r}^{\ell+1}$  ▷ Cramer's rule
9:       Error:  $\mathbf{e}^{\ell+1} = \mathbf{v}^{\ell+1} - \mathbf{u}^{\ell+1}$ 
10:    else
11:      Recursion: FAS( $\mathbf{N}^{\ell+1}, \mathbf{u}^{\ell+1}, \mathbf{S}^{\ell+1}, \nu_1, \nu_2, \ell + 1$ )
12:    end if
13:    Correction:  $\mathbf{u}^\ell = \mathbf{u}^\ell + \mathbf{I}_{\ell+1}^\ell \mathbf{e}^{\ell+1}$ 
14:    Post-smooth:  $\mathbf{u}^\ell := \text{smooth}(\mathbf{N}^\ell, \mathbf{u}^\ell, \mathbf{S}^\ell, \nu_2)$  ▷ nonlinear Gauss-Seidel method
15:  end while
16: end procedure

```

Let n be the smoothing iteration, and define

$$\begin{aligned}
M_{i+\frac{1}{2},j,k}^x &:= M \left(\frac{1}{2} A_x \phi_{i+\frac{1}{2},j,k}^\kappa - \frac{1}{2} A_x \phi_{i+\frac{1}{2},j,k}^{\kappa-1} \right), \\
M_{i,j+\frac{1}{2},k}^y &:= M \left(\frac{1}{2} A_y \phi_{i,j+\frac{1}{2},k}^\kappa - \frac{1}{2} A_y \phi_{i,j+\frac{1}{2},k}^{\kappa-1} \right), \\
M_{i,j,k+\frac{1}{2}}^z &:= M \left(\frac{1}{2} A_z \phi_{i,j,k+\frac{1}{2}}^\kappa - \frac{1}{2} A_z \phi_{i,j,k+\frac{1}{2}}^{\kappa-1} \right).
\end{aligned}$$

Then the smoothing scheme is given by: for every (i, j, k) , stepping lexicographically from $(1, 1, 1)$ to (m, n, l) , find $\phi_{i,j,k}^{\kappa+1,n+1}, \mu_{i,j,k}^{\kappa+\frac{1}{2},n+1}, \kappa_{i,j,k}^{\kappa+\frac{1}{2},n+1}$ that solve

$$\begin{aligned}
\phi_{i,j,k}^{\kappa+1,n+1} + \frac{\tau}{h^2} \left(M_{i+\frac{1}{2},j,k}^x + M_{i-\frac{1}{2},j,k}^x + M_{i,j+\frac{1}{2},k}^y + M_{i,j-\frac{1}{2},k}^y + M_{i,j,k+\frac{1}{2}}^z + M_{i,j,k-\frac{1}{2}}^z \right) \mu_{i,j,k}^{\kappa+\frac{1}{2},n+1} &= \tilde{S}_{i,j,k}^{(1)}, \\
\mu_{i,j,k}^{\kappa+1/2,n+1} - \left(\frac{1}{4} \left((\phi_{i,j,k}^{\kappa+1,n})^2 + (\phi_{i,j,k}^\kappa)^2 \right) + \frac{1-\epsilon}{2} \right) \phi_{i,j,k}^{\kappa+1,n+1} + \frac{6}{h^2} \omega_{i,j,k}^{\kappa+\frac{1}{2},n+1} &= \tilde{S}_{i,j,k}^{(2)}, \\
\omega_{i,j,k}^{\kappa+1/2} + \frac{3}{h^2} \phi_{i,j,k}^{\kappa+1,n+1} &= \tilde{S}_{i,j,k}^{(3)},
\end{aligned}$$

where

$$\begin{aligned}
\tilde{S}_{i,j,k}^{(1)} &:= S_{i,j,k}^{(1)} + \frac{\tau}{h^2} \left(M_{i+\frac{1}{2},j,k}^x \mu_{i+1,j,k}^{\kappa+\frac{1}{2},n} + M_{i-\frac{1}{2},j,k}^x \mu_{i-1,j,k}^{\kappa+\frac{1}{2},n+1} + M_{i,j+\frac{1}{2},k}^y \mu_{i,j+1,k}^{\kappa+\frac{1}{2},n} + M_{i,j-\frac{1}{2},k}^y \mu_{i,j-1,k}^{\kappa+\frac{1}{2},n+1} \right. \\
&\quad \left. + M_{i,j,k+\frac{1}{2}}^z \mu_{i,j,k+1}^{\kappa+\frac{1}{2},n} + M_{i,j,k-\frac{1}{2}}^z \mu_{i,j,k-1}^{\kappa+\frac{1}{2},n+1} \right), \\
\tilde{S}_{i,j,k}^{(2)} &:= S_{i,j,k}^{(2)} + \frac{1}{4} \left((\phi_{i,j,k}^{\kappa+1,n})^2 + (\phi_{i,j,k}^k)^2 \right) \phi_{i,j,k}^k \\
&\quad + \frac{1}{h^2} \left(\omega_{i+1,j,k}^{\kappa+\frac{1}{2},n} + \omega_{i-1,j,k}^{\kappa+\frac{1}{2},n+1} + \omega_{i,j+1,k}^{\kappa+\frac{1}{2},n} + \omega_{i,j-1,k}^{\kappa+\frac{1}{2},n+1} + \omega_{i,j,k+1}^{\kappa+\frac{1}{2},n} + \omega_{i,j,k-1}^{\kappa+\frac{1}{2},n+1} \right), \\
\tilde{S}_{i,j,k}^{(3)} &:= S_{i,j,k}^{(3)} + \frac{1}{2h^2} \left(\phi_{i+1,j,k}^{\kappa+1,n} + \phi_{i-1,j,k}^{\kappa+1,n+1} + \phi_{i,j+1,k}^{\kappa+1,n} + \phi_{i,j-1,k}^{\kappa+1,n+1} + \phi_{i,j,k+1}^{\kappa+1,n} + \phi_{i,j,k-1}^{\kappa+1,n+1} \right).
\end{aligned}$$

The above linearized system, which comes from a local Picard linearization of the cubic term in the Gauss-Seidel scheme, can be solved by Cramer's Rule.

6 Numerical results

In this section, we perform some numerical simulations for the three-dimensional scheme (3.1), to verify the theoretical results.

6.1 Convergence and complexity of the multigrid solver

In this subsection we demonstrate the accuracy and efficiency of the multigrid solver. We present the results of the convergence tests and perform some sample computations to verify the convergence and near optimal complexity with respect to the grid size h .

In the first part of this test, we demonstrate the second order accuracy in time and space. The initial data is given by

$$\phi_0(x, y, z) = 0.2 + 0.05 \cos(2\pi x/3.2) \cos(2\pi y/3.2) \cos(2\pi z/3.2), \quad (6.1)$$

with $\Omega = [0, 3.2]^3$, $\epsilon = 2.5 \times 10^{-2}$, $\tau = 0.05h$ and $T = 0.16$. We use a linear refinement path, *i.e.*, $s = Ch$. At the final time $T = 0.16$, we expect the global error to be $\mathcal{O}(s^2) + \mathcal{O}(h^2) = \mathcal{O}(h^2)$ under either the ℓ^2 or ℓ^∞ norm, as $h, s \rightarrow 0$. Since we do not have an exact solution, instead of calculating the error at the final time, we compute the Cauchy difference, which is defined as $\delta_\phi := \phi_{h_f} - \mathcal{I}_c^f(\phi_{h_c})$, where \mathcal{I}_c^f is a bilinear interpolation operator (We applied Nearest Neighbor Interpolation in Matlab, which is similar to the 2D case in [29, 31]). This requires having a relatively coarse solution, parametrized by h_c , and a relatively fine solution, parametrized by h_f , where $h_c = 2h_f$, at the same final time. The ℓ^2 norms of Cauchy difference and the convergence rates can be found in Table 1. The results confirm our expectation for the convergence order.

Remark 6.1. *When calculating the Cauchy difference between the two different grids, the interpolation operator should be consist with the discrete stencil, otherwise the optimal convergence rate may not be observed. We applied Nearest Neighbor Interpolation in Matlab.*

In the second part of this test, we investigate the complexity of the multigrid solver. The number of multigrid iterations to reach the residual tolerance is given in Table 2, for various choices of grid

Table 1: Errors and convergence rates. Parameters are given in the text, and the initial data are defined in (6.1). The refinement path is $\tau = 0.05h$.

Grid sizes	$16^3 - 32^3$	$32^3 - 64^3$	$64^3 - 128^3$
Error	2.3371×10^{-8}	5.8027×10^{-9}	1.4411×10^{-9}
Rate	-	2.0099	2.0096

sizes and (ν_1, ν_2) . Table 2 indicates that the iteration numbers are nearly independent on h , when we use 2 pre-smoothing and 2 post-smoothing. The detailed reduction in the norm of the residual for each V-cycle iteration at the 10th time step can be found in Figure 1. As can be seen, the norm of the residual of each V-cycle is reduced by approximately the same rate each time with $\nu_1 = \nu_2 = 2$, regardless of h . This is a typical feature of multigrid when it is operating with optimal complexity [47, 62, 68]. For $\nu_1 = \nu_2 = 1$, we do not observe a similar feature. Moreover, we also observe that more multigrid iterations are required for smaller values of h , which confirms our convergence analysis.

Table 2: The number of multigrid iterations of each residual below the tolerance $tol = 10^{-8}$ at the 10-th time step (i.e. at time 1.0×10^{-2} with time steps $\tau = 1.0 \times 10^{-3}$). The rest of parameters are $\varepsilon = 2.5 \times 10^{-2}$, and $\Omega = [0, 3.2] \times [0, 3.2] \times [0, 3.2]$.

$(\nu_1, \nu_2) \backslash$ Grid sizes	16	32	64	128
(1,1)	7	9	12	21
(2,2)	4	5	5	5

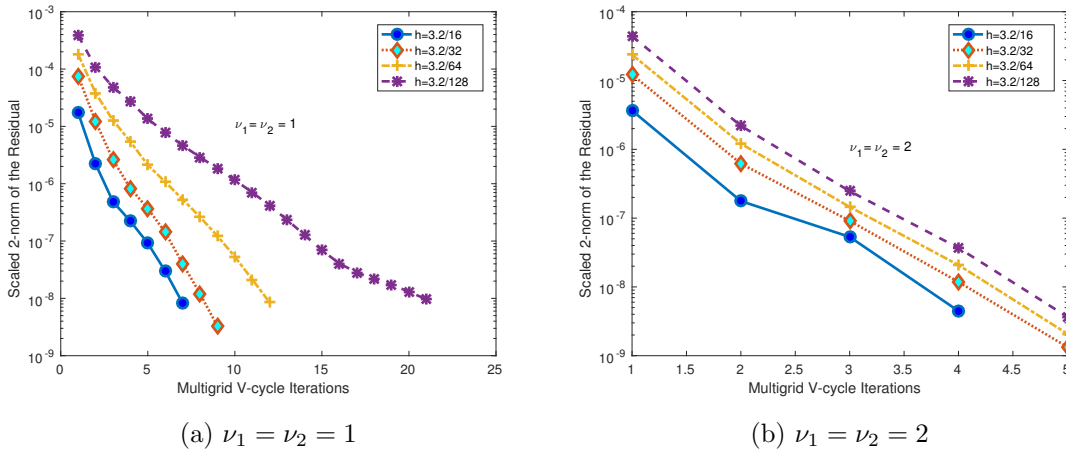


Figure 1: The reduction in the norm of the residual for each V-cycle iteration at the 10th time step (i.e. at time 1.0×10^{-1} with time steps $\tau = 1.0 \times 10^{-3}$). The rest of parameters are $\varepsilon = 5.0 \times 10^{-2}$, and $\Omega = [0, 3.2] \times [0, 3.2] \times [0, 3.2]$ and the initial condition is (6.1).

6.2 Growth of a polycrystal

The initial data for this simulation are taken as essentially random:

$$\phi_{i,j,k}^0 = 0.2 + 0.005 \cdot r_{i,j,k}, \quad (6.2)$$

where the $r_{i,j,k}$ are uniformly distributed random numbers in $[0, 1]$. Time snapshots of the microstructure can be found in Figure 2. The numerical results are consistent with the experiments on this topic in [35].

7 Conclusions

In this paper, we have provided a detailed convergence analysis of a finite difference scheme for the three-dimensional PFC equation, with the second order accuracy in both time and space established. The numerical scheme was proposed in [46], with the unique solvability and unconditional energy stability already proved in the earlier work. Meanwhile, a theoretical justification of the convergence analysis turns out to be challenging, due to a difficulty to obtain a maximum norm bound of the numerical solution in three-dimensional space. We overcome this difficulty with the help of discrete Fourier transformation, and repeated applications of Parseval equality in both continuous and discrete spaces. With such a discrete maximum norm bound developed for the numerical solution, the convergence analysis could be derived by a careful process of consistency estimate and stability analysis for the numerical error function.

In addition, we describe the detailed multigrid solver to implement this numerical scheme over a three-dimensional domain. Various numerical results are presented, including the numerical convergence test and the three-dimensional polycrystal growth simulation. The efficiency and robustness of the nonlinear multigrid solver has been extensively demonstrated in these three-dimensional numerical experiments.

8 Acknowledgments

The second author would like to thank Jing Guo at South China University of Technology for the valuable discussions. This work is supported in part by NSF DMS-1418689 (C. Wang), NSF DMS-1418692 (S. Wise), NSFC 11271048, 91130021 and the Fundamental Research Funds for the Central Universities (Z. Zhang).

References

- [1] C. Achim, M. Karttunen, K.R. Elder, E. Granato, T. Ala-Nissila, and S.C. Ying. Phase diagram and commensurate-incommensurate transitions in the phase field crystal model with an external pinning potential. *Phys. Rev. E*, 74:021104, 2006.
- [2] C. Achim, J. Ramos, M. Karttunen, K.R. Elder, E. Granato, T. Ala-Nissila, and S.C. Ying. Nonlinear driven response of a phase-field crystal in a periodic pinning potential. *Phys. Rev. E*, 79:011606, 2009.

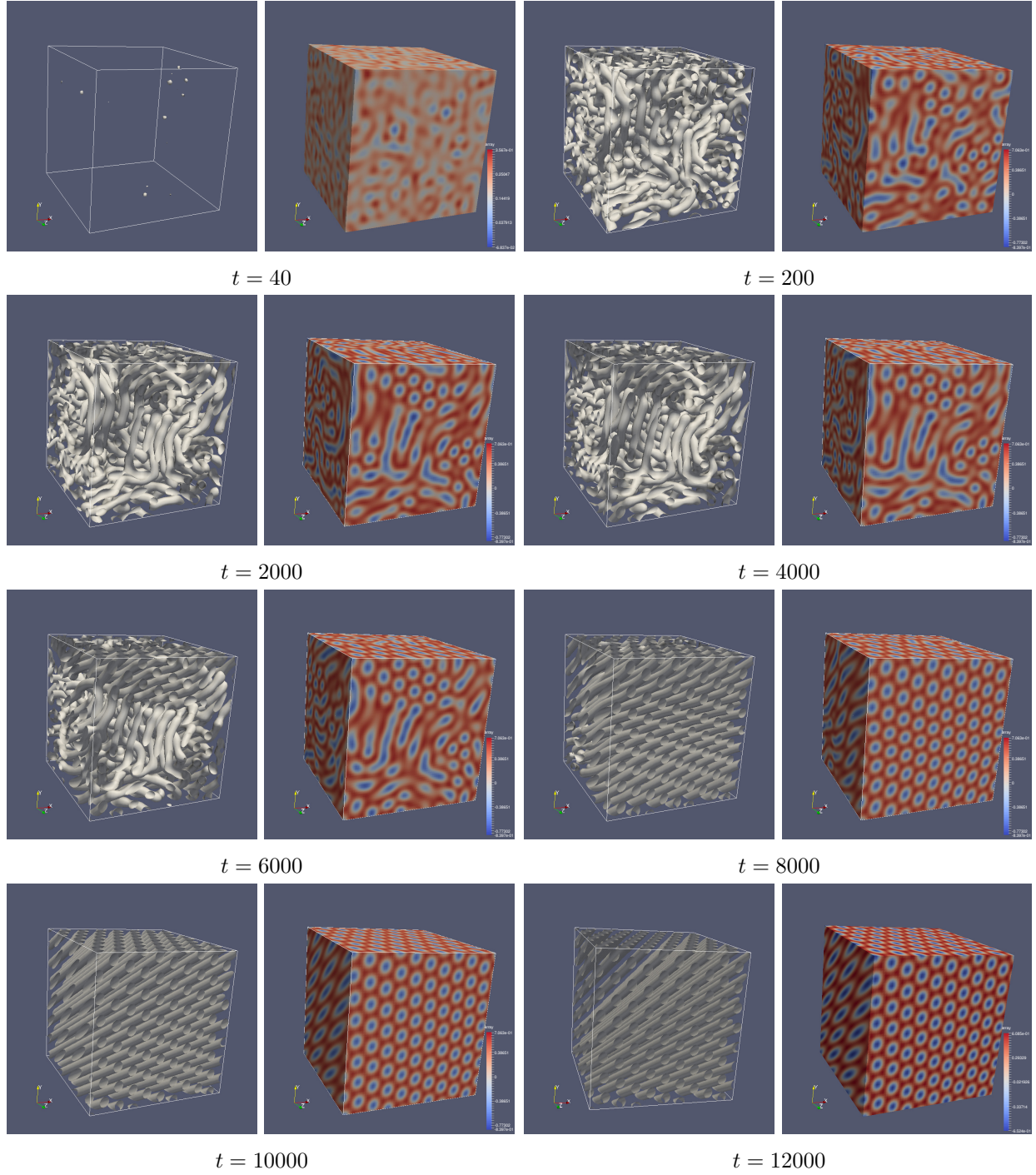


Figure 2: Three-dimensional periodic micro-structures snapshots with initial condition (6.2) at $t = 40, 200, 2000, 4000, 6000, 8000, 10000$ and 12000 . Left: iso-surface plots of $\phi = 0.0$, Right: snapshots of micro-structures plots. The parameters are $\varepsilon = 2.5 \times 10^{-1}, \Omega = [0, 64] \times [0, 64] \times [0, 64], \tau = 1.0 \times 10^{-2}$.

- [3] S. Aland, J.S. Lowengrub, and A. Voigt. Particles at fluid-fluid interfaces: A new Navier-Stokes-Cahn-Hilliard surface-phase-field-crystal model. *Phys. Rev. E*, 86(4):046321, 2012.
- [4] B. Athreya, N. Goldenfeld, and J. Dantzig. Renormalization-group theory for the phase-field crystal equation. *Phys. Rev. E*, 74:011601, 2006.
- [5] B. Athreya, N. Goldenfeld, J. Dantzig, M. Greenwood, and N. Provatas. Adaptive mesh computation of polycrystalline pattern formation using a renormalization-group reduction of the phase-field crystal model. *Phys. Rev. E*, 76:056706, 2007.
- [6] R. Backofen, A. Rätz, and A. Voigt. Nucleation and growth by a phase field crystal (PFC) model. *Phil. Mag. Lett.*, 87:813, 2007.
- [7] R. Backofen and A. Voigt. A phase field crystal study of heterogeneous nucleation—application of the string method. *Eur. Phys. J. Spec. Top.*, 223(3):497–509, 2014.
- [8] A. Baskaran, Z. Hu, J. Lowengrub, C. Wang, S.M. Wise, and P. Zhou. Energy stable and efficient finite-difference nonlinear multigrid schemes for the modified phase field crystal equation. *J. Comput. Phys.*, 250:270–292, 2013.
- [9] A. Baskaran, J. Lowengrub, C. Wang, and S. Wise. Convergence analysis of a second order convex splitting scheme for the modified phase field crystal equation. *SIAM J. Numer. Anal.*, 51:2851–2873, 2013.
- [10] J. Berry, K.R. Elder, and M. Grant. Melting at dislocations and grain boundaries: A phase field crystal study. *Phys. Rev. B*, 77:061506, 2008.
- [11] J. Berry and M. Grant. Modeling multiple time scales during glass formation with phase-field crystals. *Phys. Rev. Lett.*, 106:175702, 2011.
- [12] J. Bueno, I. Starodumov, H. Gomez, P. Galenko, and D. Alexandrov. Three dimensional structures predicted by the modified phase field crystal equation. *Comput. Mater. Sci.*, 111:310–312, 2016.
- [13] H. Cao and Z. Sun. Two finite difference schemes for the phase field crystal equation. *Sci. China Math.*, 58(11):2435–2454, 2015.
- [14] W. Chen, S. Conde, C. Wang, X. Wang, and S.M. Wise. A linear energy stable scheme for a thin film model without slope selection. *J. Sci. Comput.*, 52:546–562, 2012.
- [15] W. Chen, W. Feng, Y. Liu, C. Wang, and S.M. Wise. A second order energy stable scheme for the Cahn-Hilliard-Hele-Shaw equations. *arXiv preprint arXiv:1611.02967*, 2016.
- [16] W. Chen, Y. Liu, C. Wang, and S.M. Wise. An optimal-rate convergence analysis of a fully discrete finite difference scheme for Cahn-Hilliard-Hele-Shaw equation. *Math. Comput.*, 85:2231–2257, 2016.
- [17] W. Chen, C. Wang, X. Wang, and S.M. Wise. A linear iteration algorithm for energy stable second order scheme for a thin film model without slope selection. *J. Sci. Comput.*, 59:574–601, 2014.

- [18] M. Cheng and J.A. Warren. An efficient algorithm for solving the phase field crystal model. *J. Comput. Phys.*, 227:6241, 2008.
- [19] A. Christlieb, J. Jones, K. Promislow, B. Wetton, and M. Willoughby. High accuracy solutions to energy gradient flows from material science models. *J. Comput. Phys.*, 257:193–215, 2014.
- [20] C. Collins, J. Shen, and S.M. Wise. An efficient, energy stable scheme for the Cahn-Hilliard-Brinkman system. *Commun. Comput. Phys.*, 13:929–957, 2013.
- [21] M. Dehghan and V. Mohammadi. The numerical simulation of the phase field crystal (pfc) and modified phase field crystal (mpfc) models via global and local meshless methods. *Comput. Methods Appl. Mech. Engrg.*, 298:453–484, 2016.
- [22] A. Diegel, X. Feng, and S.M. Wise. Convergence analysis of an unconditionally stable method for a Cahn-Hilliard-Stokes system of equations. *SIAM J. Numer. Anal.*, 53:127–152, 2015.
- [23] A. Diegel, C. Wang, and S.M. Wise. Stability and convergence of a second order mixed finite element method for the Cahn-Hilliard equation. *IMA J. Numer. Anal.*, 36:1867–1897, 2016.
- [24] K.R. Elder and M. Grant. Modeling elastic and plastic deformations in nonequilibrium processing using phase field crystal. *Phys. Rev. E*, 90:051605, 2004.
- [25] K.R. Elder, M. Katakowski, M. Haataja, and M. Grant. Modeling elasticity in crystal growth. *Phys. Rev. Lett.*, 88:245701, 2002.
- [26] K.R. Elder and N. Provatas. Amplitude expansion of the binary phase-field-crystal model. *Phys. Rev. E*, 81(1):011602, 2010.
- [27] K.R. Elder, N. Provatas, J. Berry, P. Stefanovic, and M. Grant. Phase-field crystal modeling and classical density functional theory of freezing. *Phys. Rev. B*, 77:064107, 2007.
- [28] D. Eyre. Unconditionally gradient stable time marching the Cahn-Hilliard equation. In J. W. Bullard, R. Kalia, M. Stoneham, and L.Q. Chen, editors, *Computational and Mathematical Models of Microstructural Evolution*, volume 53, pages 1686–1712, Warrendale, PA, USA, 1998. Materials Research Society.
- [29] W. Feng, Z. Guan, J. Lowengrub, S.M. Wise, and C. Wang. An energy stable finite-difference scheme for Functionalized Cahn-Hilliard Equation and its convergence analysis. *arXiv preprint arXiv:1610.02473*, 2016.
- [30] W. Feng, Z. Guo, J. Lowengrub, and S.M. Wise. Mass-conservative cell-centered finite difference methods and an efficient multigrid solver for the diffusion equation on block-structured, locally cartesian adaptive grids. *In preparation*, 2016.
- [31] W. Feng, A.J. Salgado, C. Wang, and S.M. Wise. Preconditioned steepest descent methods for some nonlinear elliptic equations involving p-Laplacian terms. *arXiv preprint arXiv:1607.01475*, 2016.

- [32] X. Feng and S.M. Wise. Analysis of a fully discrete finite element approximation of a Darcy-Cahn-Hilliard diffuse interface model for the Hele-Shaw flow. *SIAM J. Numer. Anal.*, 50:1320–1343, 2012.
- [33] N. Goldenfeld, B. Athreya, and J. Dantzig. Renormalization group approach to multiscale simulation of polycrystalline materials using the phase field crystal model. *Phys. Rev. E*, 72:020601, 2005.
- [34] N. Goldenfeld, B. Athreya, and J. Dantzig. Renormalization group approach to multiscale modelling in materials science. *J. Stat. Phys.*, 125:1015–1023, 2006.
- [35] H. Gomez and X. Nogueira. An unconditionally energy-stable method for the phase field crystal equation. *Comput. Methods in Appl. Mech. Eng.*, 249:52–61, 2012.
- [36] M. Grasselli and M. Pierre. Energy stable and convergent finite element schemes for the modified phase field crystal equation. *ESAIM: M2AN*, 50(5):1523–1560, 2016.
- [37] Z. Guan, V. Heinonen, J.S. Lowengrub, C. Wang, and S.M. Wise. An energy stable, hexagonal finite difference scheme for the 2d phase field crystal amplitude equations. *J. Comput. Phys.*, 321:1026–1054, 2016.
- [38] Z. Guan, J.S. Lowengrub, C. Wang, and S.M. Wise. Second-order convex splitting schemes for nonlocal Cahn-Hilliard and Allen-Cahn equations. *J. Comput. Phys.*, 277:48–71, 2014.
- [39] Z. Guan, C. Wang, and S.M. Wise. A convergent convex splitting scheme for the periodic nonlocal Cahn-Hilliard equation. *Numer. Math.*, 128:377–406, 2014.
- [40] F. Guillén-González and G. Tierra. Second order schemes and time-step adaptivity for Allen-Cahn and Cahn-Hilliard models. *Comput. Math. Appl.*, 68(8):821–846, 2014.
- [41] J. Guo, C. Wang, S.M. Wise, and X. Yue. An H^2 convergence of a second-order convex-splitting, finite difference scheme for the three-dimensional Cahn-Hilliard equation. *Comm. Math. Sci.*, 14:489–515, 2016.
- [42] R. Guo and Y. Xu. Local discontinuous galerkin method and high order semi-implicit scheme for the phase field crystal equation. *SIAM J. Sci. Comput.*, 38(1):A105–A127, 2016.
- [43] D. Han, A. Brylev, X. Yang, and Z. Tan. Numerical analysis of second order, fully discrete energy stable schemes for phase field models of two phase incompressible flows. *J. Sci. Comput.*, 2016. Accepted and in press.
- [44] V. Heinonen, C. Achim, K.R. Elder, S. Buyukdagli, and T. Ala-Nissila. Phase-field-crystal models and mechanical equilibrium. *Phys. Rev. E*, 89:032411, 2014.
- [45] T. Hirouchi, T. Takaki, and Y. Tomita. Development of numerical scheme for phase field crystal deformation simulation. *Comput. Mater. Sci.*, 44:1192–1197, 2009.
- [46] Z. Hu, S. Wise, C. Wang, and J. Lowengrub. Stable and efficient finite-difference nonlinear-multigrid schemes for the phase-field crystal equation. *J. Comput. Phys.*, 228:5323–5339, 2009.

- [47] D. Kay and Richard Welford. A multigrid finite element solver for the Cahn-Hilliard equation. *J. Comput. Phys.*, 212(1):288–304, 2006.
- [48] U.M.B. Marconi and P. Tarazona. Dynamic density functional theory of liquids. *J. Chem. Phys.*, 110:8032, 1999.
- [49] J. Mellenthin, A. Karma, and M. Plapp. Phase-field crystal study of grain-boundary premelting. *Phys. Rev. B*, 78:184110, 2008.
- [50] S. Praetorius and A. Voigt. A phase field crystal approach for particles in a flowing solvent. *Macromol. Theory Simul.*, 20(7):541–547, 2011.
- [51] S. Praetorius and A. Voigt. A Navier-Stokes phase-field crystal model for colloidal suspensions. *J. Chem. Phys.*, 142(15):154904, 2015.
- [52] N. Provatas, J.A. Dantzig, B. Athreya, P. Chan, P. Stefanovic, N. Goldenfeld, and K.R. Elder. Using the phase-field crystal method in the multiscale modeling of microstructure evolution. *JOM*, 59:83, 2007.
- [53] J. Ramos, E. Granato, C. Achim, S.C. Ying, K.R. Elder, and T. Ala-Nissila. Thermal fluctuations and phase diagrams of the phase-field crystal model with pinning. *Phys. Rev. E*, 78:031109, 2008.
- [54] J. Ramos, E. Granato, S.C. Ying, C. Achim, K.R. Elder, and T. Ala-Nissila. Dynamical transitions and sliding friction of the phase-field-crystal model with pinning. *Phys. Rev. E*, 81:011121, 2010.
- [55] J. Shen, C. Wang, X. Wang, and S.M. Wise. Second-order convex splitting schemes for gradient flows with Ehrlich-Schwoebel type energy: Application to thin film epitaxy. *SIAM J. Numer. Anal.*, 50:105–125, 2012.
- [56] R. Spatschek and A. Karma. Amplitude equations for polycrystalline materials with interaction between composition and stress. *Phys. Rev. B*, 81:214201, 2010.
- [57] P. Stefanovic, M. Haataja, and N. Provatas. Phase-field crystals with elastic interactions. *Phys. Rev. Lett.*, 96:225504, 2006.
- [58] P. Stefanovic, M. Haataja, and N. Provatas. Phase field crystal study of deformation and plasticity in nanocrystalline materials. *Phys. Rev. E*, 80:046107, 2009.
- [59] J. Swift and P.C. Hohenberg. Hydrodynamic fluctuations at the convective instability. *Phys. Rev. A*, 15:319, 1977.
- [60] G. Tegze, G. Bansal, G.I. Tóth, T. Pusztai, Z. Fan, and L. Gránásy. Advanced operator splitting-based semi-implicit spectral method to solve the binary phase-field crystal equations with variable coefficients. *J. Comput. Phys.*, 228:1612–1623, 2009.
- [61] L.N. Trefethen. *Spectral methods in MATLAB*, volume 10. SIAM, 2000.
- [62] U. Trottenberg, C. W. Oosterlee, and A. Schuller. *Multigrid*. Academic press, 2000.

- [63] B.P. Vollmayr-Lee and A.D. Rutenberg. Fast and accurate coarsening simulation with an unconditionally stable time step. *Phys. Rev. E*, 68:066703, 2003.
- [64] C. Wang, X. Wang, and S.M. Wise. Unconditionally stable schemes for equations of thin film epitaxy. *Discrete Contin. Dyn. Sys. A*, 28:405–423, 2010.
- [65] C. Wang and S.M. Wise. Global smooth solutions of the modified phase field crystal equation. *Methods Appl. Anal.*, 17:191–212, 2010.
- [66] C. Wang and S.M. Wise. An energy stable and convergent finite-difference scheme for the modified phase field crystal equation. *SIAM J. Numer. Anal.*, 49:945–969, 2011.
- [67] A.A. Wheeler. Phase-field theory of edges in an anisotropic crystal. *Proc. R. Soc. A*, 462:3363–3384, 2006.
- [68] S.M. Wise. Unconditionally stable finite difference, nonlinear multigrid simulation of the Cahn-Hilliard-Hele-Shaw system of equations. *J. Sci. Comput.*, 44:38–68, 2010.
- [69] S.M. Wise, C. Wang, and J.S. Lowengrub. An energy stable and convergent finite-difference scheme for the phase field crystal equation. *SIAM J. Numer. Anal.*, 47:2269–2288, 2009.
- [70] S.M. Wise, C. Wang, and J.S. Lowengrub. An energy stable and convergent finite-difference scheme for the phase field crystal equation. *SIAM J. Numer. Anal.*, 47:2269–2288, 2009.
- [71] K.A. Wu, M. Plapp, and P.W. Voorhees. Controlling crystal symmetries in phase-field crystal models. *J. Phys.: Condensed Matter*, 22:364102, 2010.
- [72] K.A. Wu and P.W. Voorhees. Stress-induced morphological instabilities at the nanoscale examined using the phase field crystal approach. *Phys. Rev. B*, 80:125408, 2009.
- [73] X. Yang. Linear, and unconditionally energy stable numerical schemes for the phase field model of homopolymer blends. *J. Comput. Phys.*, 302:509–523, 2016.
- [74] X. Yang and D. Han. Linearly first- and second-order, unconditionally energy stable schemes for the phase field crystal equation. *J. Comput. Phys.*, 2016. Accepted and in press.
- [75] D.H. Yeon, Z. Huang, K.R. Elder, and K. Thornton. Density-amplitude formulation of the phase-field crystal model for two-phase coexistence in two and three dimensions. *Philos. Mag.*, 90:237–263, 2010.
- [76] Y. Yu, R. Backofen, and A. Voigt. Morphological instability of heteroepitaxial growth on vicinal substrates: A phase-field crystal study. *J. Cryst. Growth*, 318(1):18–22, 2011.
- [77] Z. Zhang, Y. Ma, and Z. Qiao. An adaptive time-stepping strategy for solving the phase field crystal model. *J. Comput. Phys.*, 249:204–215, 2013.
- [78] J. Zhao, Q. Wang, and X. Yang. Numerical approximations for a phase field dendritic crystal growth model based on the invariant energy quadratization approach. *Inter. J. Num. Meth. Engr.*, 2016. Accepted and in press.